Characterisation of immiscibility in calcium borosilicates used for the immobilisation of Mo^{6+} under Au-irradiation

Karishma B. Patel[*†], *Sophie Schuller*[∞], *Sébastien P. Facq*[†], *Ian Farnan*[†]

[†] Department of Earth Sciences, University of Cambridge, Downing Street, Cambridge, CB23EQ, UK

[∞] CEA, DES, ISEC, DE2D, Université Montpellier, Marcoule, Bagnols-sur-Cèze, France

ABSTRACT The aim of this paper was to assess factors affecting primary and secondary phase separation in simplified calcium borosilicate glasses studied for nuclear waste applications. Several glasses with varying [MoO_3] and [B_2O_3] were synthesised and exposed to Au-irradiation to examine compositional effects on the glass structure and domain size of separated phases induced by accumulated radiation damage resulting from α-decay over a ~1000 year timeframe. The produced glasses fell within the immiscibility dome of $CaO–SiO_2–B_2O_3$ and showed a unique microstructure of embedded immiscibility with three identifiable amorphous phases according to electron microscopy, Raman spectroscopy and diffraction. These glasses were then bombarded with 7 MeV Au^{3+} ions to a dose of 3×10^{14} ions/cm^2 creating an estimated ~1 dpa of damage. Several changes to the morphology, spatial distribution and size of secondary phases were observed, indicative of significant structural reorganisation and changes to the chemical composition of each phase. A general mechanism of coalescence to form larger particles was observed for [MoO_3] < 2.5mol%, while segregation to form smaller more evenly distributed particles was seen for [B_2O_3] ≤ 15mol% and [MoO_3] ≥ 2.5mol%. These microscopic changes were concurrent to surface-bulk diffusion of Ca and/or Mo ions, where the direction of diffusion was dependent on [B_2O_3] with a barrier identified at ~20mol%, as well as cross phase diffusion of said ions. These modifications occurred in part through the formation of distorted ring structures within the borosilicate network, which enabled the increased dissolution of isolated $(MoO_4)^{2-}$ units. Au-irradiation was therefore able to increase the solubility of molybdenum and alter the structure and composition of secondary phases with the extent of modification varying with [MoO_3] and [B_2O_3]/[SiO_2], though glasses notably remained heterogeneous. The collective

results suggest that radiation and composition can both be used as design tools to modulate the domain size and distribution of separated phases in heterogeneous glasses.

1.0 Introduction

The storage of nuclear waste is a complex problem, as materials are required to encapsulate a wide variety of radionuclides, show resistance to chemical leaching and radiogenic heat, in addition to maintaining structural integrity following internal decay processes [1–4]. In many countries these wasteforms will be buried in a near surface or deep geological repository (~ 500 m) for millennia [5]. This places a heavy burden on the wasteform to maintain physicochemical properties over long timescales, as nuclear waste will be radioactive for longer than several human lifetimes [6].

It is common practice to immobilize high-level waste (HLW) in a borosilicate or aluminoborosilicate matrix [6], as these amorphous structures exhibit many of these capabilities [1–3]. They can also be manufactured under reasonable temperatures and pressures, necessary for large scale industrial applications. However, waste loading is limited to ~18.5 – 20 wt% in French borosilicates and US aluminoborosilicates [7, 8], in order to prevent the uncontrolled crystallisation of molybdates, rare-earths, silicates and chromites [9–11], which can act as carriers for radioactive cesium, strontium, or minor actinides (MAs) and lanthanides (Ce^{3+}, La^{3+}, Sm^{3+}, Nd^{3+}, Gd^{3+}, Y^{3+}) [1, 12, 13]. High concentrations of molybdenum are expected from weapons-grade waste, post operative clean out, increased fuel utilization, or Generation IV reactors [1, 14, 15]. It is also a concern if increased waste loading is to be considered, as a means to minimize the final volume of waste for long-term storage. In excess, the fission product molybdenum can lead to the formation of water-soluble alkali molybdates (Na_2MoO_4, Cs_2MoO_4), known as yellow phase [12, 16].

Given that these compounds exhibit a high water solubility and can act as carriers for radioactive elements [1, 15], the formation of this complex can severely alter the chemical durability of the wasteform during long-term storage [14, 17]. In its stead, selective formation of $CaMoO_4$, which is 13,500× less soluble than alkali molybdates [18] has become of industrial interest.

In reprocessed waste streams, molybdenum will primarily be hexavalent taking the form of $(MoO_4)^{2-}$ tetrahedral units in oxidizing or neutral conditions [19–21]. According to *Greaves'* random network model for modified silicates [22] and experimental Mo EXAFS [9, 23, 24], these tetrahedral units are unconnected to each other and to the surrounding borosilicate framework, and are instead located in non-bridging oxygen (NBO) channels lined with charge balancing cations. In this configuration, these cations are octahedrally coordinated and bound to $(MoO_4)^{2-}$ entities by weak long-range ionic forces in either the glassy or crystalline phase [23, 25, 26], hence why molybdenum has a limited solubility in glasses [19].

The ability to incorporate molybdenum is dependent on the initial glass structure. An amorphous network is classically defined as a random aperiodic structure that lacks the long-range order assigned to crystals making it ideal to host a variety of nuclei of varying size and charge. There is, however, some general short and intermediate-range order within glasses that is related to the coordination and covalent bonding of network-forming atoms such as Si, B, Al or P located within an oxygen sublattice [22, 27]. These atoms typically take the form of XO_4 tetrahedral units, where X=Si, B, Al, P. These tetrahedra are connected to each other via X–O–X bridging bonds forming large chains and/or rings. In the case of silicates, the degree of polymerization is annotated by Q^n units, where n represents the number of bridging oxygen on SiO_4 tetrahedra [28]. When n is less than 4, a non-bridging oxygen (NBO) is present. In some cases these NBO sites will have a residual negative charge that requires charge compensation. This is also the case for

$(AlO_4)^-$ and $(BO_4)^-$ tetrahedral units, where X^{3+}, and thus these units require both an extra oxygen from an added alkali or alkaline earth oxide, as well as charge compensation to maintain electrical neutrality. These network forming units will also be found in their trigonal forms, where XO_4/XO_3 will have a significant effect on several glass properties [29, 30]. This outlines the complexity of borate glasses over silicate glass, where the former offers a much larger range of configurations between other network formers and modifier atoms [22]. This extends to borate-silicate mixed glasses known as borosilicates.

This introduces the second major component of glasses, which are network modifying units constituted of cations, such as alkalis, alkaline earths, or rare earths. These cations can be further divide into network modifiers, which break up the network through the creation of NBOs and therefore favour phase separation, and charge compensating network formers, which counteract the effects of immiscibility by stabilizing network formers [31, 32]. The coordination and connectivity of the network forming oxide units will determine the role of cations, and similarly the presence of cations can alter the ratio of XO_4/XO_3 ratio for X^{3+}, and therefore other properties of the glass such as viscosity and ion transport [33–36]. If the ionic bonds between network formers and cations break following an external treatment, the cations will be free to migrate and cluster in depolymerised regions of the glass. This clustering of cations can lead to phase separation [37–41] and the precipitation of complexes such as molybdates [19].

The specific speciation of a $CaMoO_4$ type molybdate complex in a borosilicate glass can be induced by composition [12, 23, 42], controlled cooling during synthesis [16], external heat treatments [43, 44], rapid quenching [16], or through redox chemistry [45, 46]. In this paper, composition will form the primary point of interest with a focus on factors affecting the competitive charge balancing of

network forming $(BO_4)^-$ and network modifying $(MoO_4)^{2-}$ anionic entities by a limited cation content, as this can significantly effect phase separation tendencies [47]. In soda lime borosilicates, both of these anionic units prefer Na^+ as charge balancers, but $(BO_4)^-$ network units will have a stronger affinity to this ion thus enabling the incorporation of Ca^{2+} into molybdate complexes [9, 19]. Previous studies have found that an increase of $[B_2O_3]$ or [CaO] will promote the formation of $CaMoO_4$ over Na_2MoO_4 crystallisation, as it affects the population of $(BO_4)^-$ species [12, 47]. However, the concentration of CaO in soda lime borosilicate glasses has typically been limited to < 11mol%, as it is known to cause liquid-liquid phase separation in borosilicate glass [12, 15, 48]. This limitation has resulted in Na_2MoO_4 production in most studies, despite the manipulation of the other listed factors affecting speciation [12, 21].

For this reason, Na_2O was excluded from this study even if that resulted in multi-phased glasses. This was performed as a means to isolate the key components of $CaMoO_4$ formation, and to better understand the principles of phase separation as a function $[B_2O_3]$ and $[MoO_3]$, in addition to factors affecting the solubility limit of molybdenum within matrices containing varying proportions of network formers (borate and silicate units). It further sought to examine how the glass chemistry would affect structural evolutions induced by radiation damage as a metric for long-term performance and at the same time to assess if internal radiation could be used to create a desired structural configuration.

Materials used for the storage on nuclear waste will continuously undergo internal damage from α-decay of minor actinides and Pu, β-decay of fission products, and transitional γ-decay. These processes will trigger atomic displacements, ionization, and electronic excitations, which can result in changes to the short- and medium-range ordering within the glass structure. While the former is induced by changes to the coordination of atoms resulting from a modification in

charge compensation, the latter will result from changes to bond angles between network formers and the distribution of ring sizes [49, 50]. These modifications can subsequently lead to changes in volume (swelling or densification), and mechanical properties (hardness, elasticity and fracture toughness). It can also induce phase transformations, such as devitrification, precipitation, bubble formation, glass-in-glass phase segregation, or the clustering of cations [6, 49, 51–54]. These effects will be predominantly of interest under the scope of multi-phased structures as the $[SiO_2]/[B_2O_3]$ and concentration of cations has also been observed to alter bond angles and the domain size of separated phases [34, 55–57]. Therefore, radiation may accelerate or remediate the effects of composition on glass order and subsequently phase specific properties.

During encapsulation, the α-decay process and specifically the heavy recoil nuclei are responsible for the bulk of these modifications according to both experimental work and to molecular dynamics (MD) simulations [6, 49]. During α-decay, a α (or He^{2+}) particle is ejected from a parent isotope. This small α-particle typically has a kinetic energy between 4.5 to 5.5 MeV and will travel 10 to 20 μm before stopping due to interactions with electrons in a glassy matrix [6]. The decay process will also produce a daughter isotope (parent isotope – He^{2+} particle), which is referred to as the heavy α-recoil. This isotope will have a relatively smaller kinetic energy around 70 to 100 keV, and will interact primarily through nuclear (or elastic) collisions. These nuclear interactions will cause a chain reaction that creates a dense displacement cascade, resulting in around ~ 1500 atomic displacements after travelling ~ 30 nm [6]. In order to specifically replicate the damage produced from these overlapping displacement cascades on an accelerated timescale, external radiation using medium-energy ions can be used [49, 58, 59].

Previous research has shown that borosilicate glasses subjected to internal or external irradiation have primarily remained amorphous [6, 49], with a saturation in changes to mechanical

properties, internal energy, and density observed for a cumulative dose of 4×10^{18} α/g [49, 60, 61], where an equilibrium between damage creation and thermal annealing from overlapping ion tracks occurs [49, 60]. Given current waste loading standards and waste streams, this saturation in structural modifications is expected to occur following 1000 years [6, 49], which corresponds to approximately 1 displacement per atom (dpa) [59, 60]. Using this information, experiments can be designed to simulate a maximum damage state, which can be used as a tool to reverse engineer a desired starting encapsulating medium.

This paper principally sought to identify if irradiation simulating the damage from α-decay would: 1) affect the solubility of molybdenum and potentially cause the formation of $CaMoO_4$; 2) promote phase separation in the borosilicate network; or 3) alter existing separated phases thereby affecting immiscibility tie lines, similar to temperature-based effects. In this context, solubility refers to the inclusion of isolated $(MoO_4)^{2-}$ tetrahedron within the borosilicate network, versus those that are clustered together in depolymerised areas of the glass that can serve as precursor environments for crystallisation [19, 62, 63]. Additionally, the terminology for phase transitions refers to both those between amorphous and crystalline phases, and between multiple amorphous phases that are compositionally and structurally different based on network connectivity.

2.0 Experimental procedures

2.1 Composition and synthesis technique

Multiple compositional series were created with varying $[B_2O_3]$ and $[MoO_3]$ to study the solubility and phase separation tendencies of molybdenum in calcium borosilicate base glasses, and to explore how separated phases were modified when exposed to external radiation that

displaced each atom. The first series (labelled CB) has an increasing [B_2O_3] for a fixed [SiO_2]/[CaO] ratio and MoO_3 content. This series was used to determine how the ratio of network formers altered the glass structure and phase specific properties. These samples also contained a fixed amount of rare-earth dopant, which can be considered an actinide surrogate, and can therefore indicate potential incorporation sites of radioactive elements.

The second series (labelled CM) focused on increasing the molybdenum content in simplified calcium borosilicates normalised to French nuclear waste glass SON68 (non-active form of industrial R7T7). It was used to assess the mechanism of MoO_3 incorporation and to test solubility limits, in addition to understanding how encapsulation would be affected by atomic displacements. See Table 1 for the batch compositions within these series. Owing to the heterogeneous nature of the samples it was difficult to confirm the experimental composition, but energy dispersive x-ray spectroscopy (EDS) and ^{11}B MAS NMR were used for this purpose in so far as it was possible [64, 65] (see Supporting Information).

Note that while changes to [MoO_3] and [B_2O_3] are referred to throughout the text, molybdenum will take the form of $(MoO_4)^{2-}$ complexes unconnected to the glass network, as previously mentioned. Similarly, boron will be found as BO_3 or $(BO_4)^-$ structural units that are connected to other borate or silicate units. While different fractions of tri-fold and tetra-fold co-ordinated boron will alter connectivity and properties of the glass, they are often lumped together for the purposes of this investigation owing to the complexity of these multi-phase glasses. This study thus remarks on the general effect boron oxide has on the structure of these series of glasses.

Glass batches of 30 g were prepared by milling powders of SiO_2, H_3BO_3, $CaCO_3$, MoO_3 and Gd_2O_3, followed by melting in a platinum-rhodium (90/10) crucible at 1500°C. Mixed powders were melted for 3 h, before crushing and re-melting glasses for 2h. A double melt and

variance in melt time was used to try and ensure homogeneity of element distribution, but all calcium borosilicate compositions remained multi-phased despite various techniques to increase the quench rate and induce mixing at high temperature [64]. Due to the high viscosity of these samples they needed to be quenched in a water bath and tapped out with a hammer. Fragments from this process were annealed for 24 h at 520°C to reduce minor internal stresses. They were then cut to fit the irradiation sample holder (4 mm × 4 mm) and hand polished successively using P600, 800, 1200, 2400 and 4000 SiC grit paper, followed by 3 μm and 1 μm diamond polishing to achieve a uniform thickness of approximately 500 μm.

2.2 Irradiation experiment

Energetic ions can be used to replicate the effects of various irradiation processes, such as neutron damage, β-decay, γ-decay, or α-decay [6, 66, 67]. The α-decay process is unique in that it will have both electronic of nuclear components, which can be replicated using certain ions and energies. The nuclear stopping power resulting from slow heavy ion irradiation, such as Pt, Au, and Pb ions, is similar to that of the α-recoil (5 keV/nm) [58]. Therefore, external radiation experiments of this design can reasonably replicate the damage produced by displacement cascades arising from ballistic events.

This radiation experiment was conducted at CSNSM using 7 MeV Au^{3+} ions at a flux of 2×10^{10} ions/cm^2·s based on a target current of 0.15 mA on the ARAMIS beamline. A dose of 3×10^{14} ions/cm^2 was achieved creating approximately 1 dpa. The ion penetration depth was correspondingly estimated to be ~1.6 μm, based on TRIM calculations [59] (see Electronic Supplementary Information). This degree of damage can be used to assess the structural modifications within the glassy phase(s) when every atom has been displaced, and whether this

will affect the solubility of molybdenum.

2.3 Characterization techniques

The initial microstructure of synthesised samples often contained two to three phases, either a crystalline and glass phase, or three compositionally different glass phases. As a result, multiple analytical techniques were required to assess the modifications to structure induced by irradiation. As the irradiation volume is small, characterization was limited to surface analysis using accessible techniques that would describe the short- and medium-range order of each phase.

The multi-phase glasses and glass ceramics presented varying morphologies and phases for quantification, which were analysed using Scanning Electron Microscopy (SEM) backscattered (BSE) imaging and energy dispersive x-ray spectroscopy (EDS). These were performed on a Quanta-650F held at low vacuum (0.06 – 0.08 mbar) with a 5 – 7.5 keV beam, resulting in a penetration depth of 1 μm. EDS measurements were collected with an additional 8 mm cone, to reduce skirting effects, thus providing information on the interface between phases, and the relative composition of each identifiable phase. Images were collected using FEI Maps software, while acquisition and analysis for EDS was performed using Bruker ESPRIT software from 10 – 20 mapped areas.

While electron microscopy was useful for investigating the microstructure of these complex glasses, Raman spectroscopy was used to determine bonding configurations. This was particularly useful in identifying the characteristic medium-range order of each amorphous phase. A Horiba Jobin Yvon LabRam300 spectrometer with a 300 μm confocal hole, coupled to a Peltier cooled front illuminated CCD detector with a holographic grating of 1800 grooves mm^{-1}

was employed. It utilised a diode-pumped solid-state laser (Laser Quantum) with an incident power of 100 mW focused with an Olympus 50× objective to produce a 532 nm excitation line. Spectra were collected over a 150 – 1600 cm^{-1} range with a 2 μm spot size, which resulted in a spectral resolution of ~1.4 cm^{-1} per pixel (1024 × 256 pixels in size). Multiple acquisitions (3 - 4) were made for each phase within each sample.

While most of the compositions in this study were glasses, X-ray diffraction (XRD) was primarily used to confirm this was true in the observed heterogeneous structures, and to identify any molybdate formation. A Bruker D8 ADVANCE spectrometer using $CuK_{\alpha 1}$ (λ = 0.15406 nm) equipped with Göbel mirrors for a parallel primary beam, and a Vantec position sensitive detector was enlisted for this purpose. Acquisitions were made over the 2θ = 10 – 90° spectral range with a 0.02° step size, and a 10 s per step dwell time, resulting in a ~10h run per sample.

3.0 Results

3.1 Microstructure

The microstructure of synthesised calcium borosilicate glasses in the CB and CM series showed embedded immiscibility with three identifiable phases prior to irradiation as a result of compositions falling under the immiscibility dome in the SiO_2–B_2O_3–CaO system [48]. The residual matrix is Si-rich and referred to as phase A. Within this phase there are several large droplets rich in Ca/Mo referred to as phase B. These regions of phase B are found to form in varying sizes, and are randomly distributed within phase A. Within phase B there are smaller droplets of a glassy phase that is compositionally a mixture of phases A and B [64]. These droplets are referred to as phase C and are found in an array of geometries. The most common of which are referred to as spherical, distended (a sphere with rounded protrusions), and spatters (resembles the shapes

created by paint splatters). A schematic of these heterogeneous structures and their terminology can be seen in Figure 1. Owing to the complex nature of these heterogeneous structures, changes following irradiation focused on making comparisons to the morphology, size and distribution of phase C within phase B.

While this general structure of embedded immiscibility within amorphous phases was observed in most of the samples, variations in size, distribution and morphology of phase B and phase C deposits could be observed in the CB and CM series. In the CB series, phase B deposits are initially found to form in small (2–18 μm) and medium (75–150 μm) sizes. As [B_2O_3] increases, the number of phase B deposits increases and larger deposits (> 200 μm) could also be observed. This result suggests that phase B is a carrier for boron.

Within these deposits, the distribution and number of phase C droplets also altered as [B_2O_3] increased. At low [B_2O_3], phase C droplets primarily in a spattered morphology were found to be ~3 – 18 μm in diameter, but as the regions of phase B grew with increasing [B_2O_3], so too did the size of phase C droplets forming those up to 50 μm in diameter in an increasingly spherical morphology. This change in the size range of phase C droplets was concurrent to a shift in the distribution of phase C within phase B. As [B_2O_3] increased, phase C droplets were found to form closer to the A–B interface and these droplets were larger in size compared to those in the centre of phase B.

Following Au-irradiation, the morphology of the spattered phase C droplets started to coalesce into a spherical geometry for [B_2O_3] ≤ 15mol% (see Figure 2). This was most pronounced in the centre of phase B where the average diameter of phase C droplets also decreased by ~1/3 of the original size. Comparatively, the sample with [B_2O_3] > 15mol%

showed a dispersion of spherical droplets towards that of a spattered morphology. This was particularly evident near the A–B interface as Figure 2 (d) illustrates.

After synthesis, phase B deposits in the CM series changed morphology from ellipsoidal to spherical as [MoO3] increased. These deposits also experienced a marginal increase in size with increasing [MoO3]. This observation suggests either that phase B acted as a carrier for Mo, in addition to boron and Ca ions, or that MoO_3 induced further phase separation of network formers resulting in larger separated deposits. In terms of phase C, there was a small increase of ~ 10 μm in the size distribution with increasing [MoO3], with larger droplets similarly being found near to the A–B interface. For compositions with [MoO_3] > 2.5mol%, phase B became a powellite phase with crystallites forming clusters embedded in a residual amorphous phase.

Following Au-irradiation, the sample without MoO_3 (CaBSi) showed several changes to the size and distribution of phase C deposits within phase B (see Figure 3). Firstly, there was the formation of a belt of small deposits (< 4μm) close to the A–B interface. Secondly, the size of the remaining phase C droplets increased to ~ 5 – 40μm in diameter. Thirdly, these newly formed larger droplets appeared to be undergoing a process of dispersion, following an initial coalescence of smaller droplets. This suggests that modification to separated phases may be dose dependent.

Once MoO_3 was introduced into the system, the effects of irradiation varied depending on [MoO_3]. For low [MoO_3] the formation of larger phase C deposits up to a diameter of ~ 50μm, similar to that seen in CaBSi, was observed (see Figure 4). As [MoO_3] increased to CM2.5, phase C droplets are observed to experience a significant reduction in size, with most droplets found to be < 5μm, as Figure 5 indicates. These droplets also appeared to become more evenly

distributed within phase B. These collective observations indicate a possible threshold at 1< [MoO_3] < 2.5mol% where the mechanism of alteration shifts from coalescence to dispersion of phase C droplets.

When [MoO_3] increased to 7mol%, the system shifted from being one of embedded immiscibility with three amorphous phases to that of a glass ceramic (GC) with heterogeneously distributed $CaMoO_4$ crystal clusters within a residual amorphous network. This was determined by XRD, which confirmed the formation of $CaMoO_4$ and by BSE imaging, which showed only two phases. Following irradiation very few alterations can be seen with regards to the morphology or distribution of crystal clusters (see Figure 4), indicating stability and radiation resistance to the microstructure of this GC.

3.2 Compositional changes

Given that several changes to the microstructure of these glasses were observed, EDS analysis was used as a supplementary tool to discover how some of these modifications took place, and if a correlation between morphology and composition could be drawn. Table 2 summarizes the bulk [Si]/[Ca] and [Ca]/[Mo] ratios calculated per phase based on analysis of 5-15 selected areas of mapped samples (see Figure 6 and Electronic Supplementary Information for additional maps).

To gain insight on the location of molybdenum and the mechanism of phase separation prior to irradiation these two ratios were combined to yield [Si]/[Mo] trends (see Figure 7). These trends suggest that cooling of glass melts led to the formation of phase A enriched in SiO_2 and depleted in MoO_3 (high [Si]/[Mo]), in contrast to phase B enriched in MoO_3 and depleted in SiO_2 (low [Si]/[Mo]). This later observation is likely owing to the low solubility of MoO_3 in SiO_2. Phase C,

which is a product of secondary phase separation within phase B, is richer in SiO_2 than phase B and more enriched in MoO_3 than phase A.

Following Au-irradiation, the [Si]/[Ca] ratio was generally observed to decrease and the [Ca]/[Mo] ratio to increase for $[B_2O_3] \leq 15$mol%, suggesting a bulk-to-surface diffusion of Ca. However, the rate of change was different for each phase suggesting a secondary process of cross phase diffusion. This is supported by an increase of [Si]/[Mo] in phase A, and a decrease in phase B or C identifying diffusion of Mo units. The opposite trends were observed for $[B_2O_3] >$ 15mol%, suggesting that $[B_2O_3]$ has a significant directional impact on the radiation induced diffusion of atoms. These observations can also be correlated to the shift of morphological changes observed for phase C in $[B_2O_3] \leq 15$mol% (droplet coalescence) and $[B_2O_3] >$ 15mol% (droplet dispersion).

While Table 2 provides insight into the bulk properties of each phase, properties across the interface are also of interest in order to explore the mechanism of alteration following Au-irradiation. Figure 8 illustrates the trends across the phases in CB23. Prior to irradiation the [Ca]/[Mo] ratio initially increases as we move away from the A–B interface and into phase B, and it decreases as we move into phase A. This implies a relatively Ca-rich layer on the B-side of the interface, and a Mo-rich band on the A-side. Further towards the centre of phase B, the [Mo] increases, while the [Si]/[Ca] remains fairly constant. In contrast, [Ca] decreases in phase A with distance from the A–B interface, and to a less extent so too does [Mo].

Following irradiation, the magnitude of ratios and the slope of trends change. The results in Figure 8 indicate that Mo ions move from the bulk of phase A and C to phase B. This reduces the discrete boundary between phases and the accumulation of either Ca or Mo ions along the interface. This may be related to the greater morphological changes observed near to the A–B

interface. Moreover, while [Ca] is primarily observed to decrease at the surface, relative changes to the slope of trends also imply a similar cross phase diffusion of Ca ions, though the diffusion of Mo ions out of phase C is more significant. The significant compositional changes in and around phase C are of importance given the significant morphological changes observed following irradiation.

While the general mechanisms of diffusion in the CM series were similar to the CB series as discussed above, the effect of [MoO_3] caused directional changes to the diffusion of atoms. Prior to irradiation, introducing MoO_3 to a calcium borosilicate caused Ca ions to move from phase B to phase A. As [MoO_3] increased to 2.5mol%, a reversion of trends was observed with Ca ions moving from phases A and C towards phase B. This coincided with a cross sample increase of [Mo], with the most significant changes seen in phase B, and to a somewhat lesser extent in phase C. This suggests that 1mol% MoO_3 can be incorporated in multiple phases within calcium borosilicates aided by the diffusion of Ca ions into the SiO_2 rich phase, but as [MoO_3] increases it selectively accumulated in a single phase (B), which encourages additional phase separation marked by Ca diffusion. When [MoO_3] was increased to 7mol% a GC was formed. This resulted in Ca and Mo ions being pulled out of phase A and towards crystal clusters, for which phase B acts as a precursor.

Following Au-irradiation, CaBSi showed signs of Ca diffusion from phase B towards phases C and A, as Table 2 indicates. Once MoO_3 was introduced into the system, the primary mechanism of alteration following irradiation became a surface-to-bulk diffusion of both Ca and Mo ions, with a predominance of change observed in phase A. As [MoO_3] increased to 2.5mol%, Ca diffusion followed a pattern similar to that which was seen in CaBSi, with Mo diffusion

following a parallel pathway. This occurred alongside a surface-to-bulk diffusion of Ca and Mo ions that was similarly observed in both CM1 and CB23.

These observations suggest two primary points of interest. The first is that as [MoO_3] increases to 2.5mol% and both Ca and Mo ions accumulate in phase B, irradiation causes the cross phase diffusion of atoms to behave in a similar manner to a glass without molybdenum. The second is that [B_2O_3] appears to be the controlling factor in surface-bulk directional diffusion independent of [MoO_3] with the following relationship:

$$\left[B_2O_3\right]: CB7 < CB15 < CM7 < CM2.5 < CM1 < CB23$$

$$\text{bulk-to-surface} \leftarrow | \rightarrow \text{surface-to-bulk}$$

Note that CB15 < CM2.5 < CB23 have a fixed [MoO_3], but that the relationship holds for 1mol% ≤ [MoO_3] ≤ 7mol% with a change in the surface-bulk diffusion direction at ~20mol% B_2O_3.

3.3 Raman analyses

In order to gain additional insight on the role of network formers and network modifying ions Raman spectroscopy was utilised. The glasses in this study showed several characteristic bands attributed to the Si-O-B structure, and to the molybdenum local environment with a dependence on composition and phase (see Figures 7-9). Across all multi-phase glasses, phase A had several bands that are typical of silicate and borate-based glasses. The most easily identifiable is the *R* band (~ 450 cm^{-1}) attributed to mixed Si-O-Si and Si-O-B bending and rocking [60, 68–70], as well as B-O-B rocking (~ 500 cm^{-1}) [71]. Additionally, there were two defect bands, D^1 and D^2, which are assigned to four-membered and three-membered SiO_4 rings, respectively. Silicate-type structures also produced overlapping bands between 850 and 1250 cm^{-1} that represent Si-O stretching vibrational modes for Q^n units [31]. Furthermore, there was a supplementary weak band at ~ 800

cm^{-1} assigned to O-Si-O symmetric bond stretching associated with Si motion against its surrounding oxygen cage [30, 69, 72]. This latter band often overlapped with a sharp peak at ~ 807 cm^{-1} attributed to the symmetric vibrations of 6-membered BO_3-triangles in boroxyl rings [69, 72–74].

In addition to broad bands characteristic of the borosilicate network, there were several additional sharp Raman bands attributed to the internal vibrations of $(MoO_4)^{2-}$ in a powellite type structure with C_{4h} point symmetry. They are the $\nu_1(A_g)$ 878 cm^{-1}, $\nu_3(B_g)$ 848 cm^{-1}, $\nu_3(E_g)$ 795 cm^{-1}, $\nu_4(E_g)$ 405 cm^{-1}, $\nu_4(B_g)$ 393 cm^{-1}, and $\nu_2(A_g+B_g)$ 330 cm^{-1} vibrational modes, which represent symmetric elongation of the molybdenum tetrahedron, asymmetrical translation of double degenerate modes, and symmetric and asymmetrical bending, respectively [75, 76]. There was an additional band around ~ 910 – 920 cm^{-1} associated with the symmetric stretching vibrational mode of $(MoO_4)^{2-}$ units dissolved in amorphous systems [21]. This collection of $(MoO_4)^{2-}$ vibrational modes can be seen in compositions with high $[MoO_3]$ and $[B_2O_3]$, or in the Mo-rich phase B.

Prior to irradiation, introducing MoO_3 to CaBSi caused growth of the O-Si-O stretching, D^2 defect, and Q^2 bands (see Figure 9), indicating that molybdenum entities create distorted ring structures and cause depolymerisation in the SiO_2 network. Increasing $[MoO_3]$ further in the CM series resulted in the formation of $(MoO_4)^{2-}$ vibrational bands. This coincided with growth of the sharp bands associated with boroxyl rings, and O-Si-O stretching, indicating further phase separation and distortion of the borosilicate network into borate-rich and silicate-rich regions. It is worth noting that $(MoO_4)^{2-}$ vibrational bands can be observed in samples with and without crystallisation. While CM7 is a GC, CM1, CM2.5, CB7, CB15 and CB23 are fully amorphous according to XRD. Therefore, as previous works have indicated, it is predicted that $(MoO_4)^{2-}$ groups are found in a similar environment whether in the amorphous or crystalline phase [21, 23],

and thus produce similar vibrations, however these bands narrow as the system becomes crystalline.

Following Au-irradiation, several structural modifications are observed for samples in the CM series. Primarily, the *R* band is observed to shift to higher wavenumbers for all multi-amorphous phased samples. This shift indicates a reduction in the inter-tetrahedral angles between network formers, implying the formation of smaller or distorted ring structures. This occurs alongside a marginal growth of the D^1 and D^2 defect bands for samples with no or low [MoO_3], which further supports the formation of smaller Si-type ring structures. In CaBSi, there was also growth of Q^3 relative to Q^2 in phase A and B, indicating an increase in the general degree of silica polymerization across all phases following radiation exposure. An opposing affect has been observed to occur in irradiated sodium borosilicate glasses [49, 60], which suggests that Ca^{2+} can reduce the population of non-bridging oxygens (NBOs), while Na^+ promote their formation following irradiation.

For samples with [MoO_3] ≥ 2.5mol%, spectral changes were predominately associated with $(MoO_4)^{2-}$ vibrational modes, and the boroxyl ring band. In CM2.5 most $(MoO_4)^{2-}$ vibrational modes within phase A (see Figure 9) and phase B (see Electronic Supplementary Information for additional spectra) could not be seen following irradiation. In their place, growth of the band associated with isolated $(MoO_4)^{2-}$ units in the amorphous network grew. This occurred alongside growth of the D^1 defect and damping of the O-Si-O stretching band, while little change to the boroxyl ring band was observed. In contrast, only minor damping of the $(MoO_4)^{2-}$ bands were observed in CM7 where $CaMoO_4$ crystallites were detected. In this composition the most significant change was a damping of the boroxyl ring band, suggesting radiation-induced ring cleavage. The collective results suggest that Au-irradiation can significantly alter the

molybdenum environment and increase dissolution of isolated $(MoO_4)^{2-}$ units through Si-O-B ring distortion, but only when $CaMoO_4$ crystallisation has not occurred.

In compositions with a fixed $[MoO_3]$, increasing $[B_2O_3]$ caused an intensity increase of the D^1 defect, concurrent to damping of the D^2 defect prior to irradiation (see Figure 10). This coincided with a sharp growth in the band associated with boroxyl rings, and with $(MoO_4)^{2-}$ vibrational modes. This result suggests that increasing $[B_2O_3]$ increased the order of $(MoO_4)^{2-}$ units towards a crystalline phase, while promoting phase separation within the borosilicate network through the formation of single atom type rings. This effect was more pronounced in phase B, which further supports the statement that B_2O_3 preferentially separates into phase B, hence why characteristic bands of silicate-based features become less significant in this phase.

Following irradiation, the $(MoO_4)^{2-}$ vibrational bands are observed to broaden within all phases, and within phase A to dampen significantly, as Figure 10 illustrates. This band broadening and damping occurred alongside growth of the band at ~ 910 cm^{-1} attributed to $(MoO_4)^{2-}$ units dissolved in the amorphous network, suggesting increased solubility of molybdenum units and the prevention of molybdate crystallisation from ordered environments. While this shift occurred in both phases A and B, the amplitude of these bands suggest that molybdenum is predominantly found in phase B. Changes to the *R* band, D^1 and D^2 defects, and O-Si-O stretching were similar to those observed in the CM series following irradiation with an exception seen for CB23. While the boroxyl band was persistent for glasses with MoO_3 in the CM series, a minor damping of this band was observed for CB23 following irradiation. This occurred alongside damping of the D^1 defect. These results indicate that Au-irradiation is more easily able to cleave smaller single atom type rings and induce the formation of larger Si-O-B ones for compositions with $[SiO_2]/[B_2O_3] < 2.8$.

Although some phase specific trends are shown in Figure 10, a large variation in structural features was actually observed by Raman spectroscopy following Au-irradiation. The spectra for CB15 in Figure 11 illustrate this point. This variance in bands can be used to gain insight into possible mechanisms of phase separation or reintegration, as these spectra were collected across phases.

Whilst general modification to the *R* band, D^2 defect and boroxyl ring bands remained similar across the spectra, the proportion of $(MoO_4)^{2-}$ vibrational modes to these bands changed. This result suggests clustering and increased order of $(MoO_4)^{2-}$ oxyanions within some localized areas, while increased dissolution of isolated units in other areas. Therefore, it can be deduced that Au-irradiation created several mixed regions within the amorphous network that showed characteristic bands of phases A and B, or of phases B and C. The predicted mixing between phases represented by these new spectra is supported by change to the microstructure of samples, and cross phase ion diffusion suggested by EDS analysis in Table 2.

4.0 Discussion

It is evident from the complex microstructures observed in this study that these borosilicate glasses underwent liquid-liquid phase separation during synthesis. This resulted in a unique heterogeneous glass for investigation. While a multi-phase glass is unconventional for industrial applications, the chosen compositional range was used to: 1) identify factors influencing molybdenum solubility and the process of $CaMoO_4$ formation, and 2) study the compositional impact on immiscibility properties at a fundamental level when the materials were subjected to Au-irradiation, which replicated the ballistic collisions from α-decay on a geological timescale.

4.1 Evolution of separated phases

Glasses are by nature non-equilibrium materials where material properties are dependent on composition and environmental factors such as temperature, pressure or high-energy events like irradiation damage [77]. These external factors can have substantial impacts on the structural components that define short-range order within the glassy matrix, especially in the case of irradiation where interactions create ballistic motion of atoms, significant heat, as well as an input of charge.

In this study, structural modifications following irradiation were most evident in phase C, where several changes to the morphology, size and spatial distribution of droplets was observed. The mechanism of alteration appeared to be dependent on composition. At low [MoO_3], phase C droplets were observed to coalesce into larger particles that became spherical, similar to the changes seen in the calcium borosilicate without MoO_3. This type of mechanism is similar to temperature-based relaxation and particle growth during cooling above T_g, and can be translated to growth of the domain size in phase separated amorphous materials [45, 57, 78–80].

Increasing [MoO_3] to 2.5mol% had an opposing effect on microstructural modifications, where separation and segregation of phase C droplets was the main mechanism of alteration. This was evident from a reduction in the size of phase C droplets that also appeared to be more evenly distributed within phase B. This type of mechanism is similar to the disorder created by irradiation in organised systems like crystals [81–83]. This type of segregation and distribution was also observable for compositions with [B_2O_3] $\leq$ 15mol%. A schematic summarizing these transformations as a function of composition can be seen in Figure 12.

The observed changes to morphology can be attributed to two factors. The first being the initial state of synthesised samples. Thermodynamically, immiscibility in glasses is controlled by the free energy of mixing, and occurs when the entropy of phase separation is lower than that of a

homogeneous state [79]. This happens when the system falls below a characteristic temperature, referred to as the phase separation temperature T_{PS}. Composition can affect this threshold, with both network formers (SiO_2, B_2O_2, and Al_2O_3) and network modifiers (alkali and alkaline earths) having an impact [84]. In a binary SiO_2–B_2O_2 system, low [B_2O_3] will induce phase separation unless a high temperature of synthesis and rapid quenching technique are used [72]. Similarly inclusion of an alkali or alkaline earth at low concentrations will induce the segregation of cation/borate-rich domains in a residual Si-rich matrix, with the regions of immiscibly increasing as the atomic number decreases [56, 85, 86]. In this set of experiments varying the melt temperature, time at temperature or quench rate did not induce homogeneity, indicating that external parameters cannot always remediate the chemical immiscibility induced by composition, or at least not within feasible laboratory ranges.

Furthermore, the inclusion of MoO_3 into these types of phase separated glasses will further promote the separation of these two domains with molybdenum favouring the borate-rich phase in SiO_2–B_2O_2–Na_2O glasses [45, 62]. This has been quantified to a ~50°C increase in T_{PS} per 0.5 mol % MoO_3 [12]. It can be assumed that MoO_3 inclusion causes an analogous increase in T_{PS} for the SiO_2–B_2O_2–CaO system [64]. This inference is based on the observations that increasing [MoO_3] increased the size phase B domains, as well as [Mo] in this phase relative to phase A. Additionally, increasing the incorporation of MoO_3 caused the formation of boroxyl rings, increased the ordering of $(MoO_4)^{2-}$ oxyanions towards a crystalline precursor, and caused a reduction in the coordination of boron [65, 87]. All of these observations point to higher T_{PS} that would increase $\Delta T = T_{PS} - T_g$ and therefore the relaxation time for a fixed cooling rate. Similar observations were seen for increasing [B_2O_3], which indicates that this too can increase T_{PS}.

In this system of embedded immiscibility secondary phase separation also occurred. It is predicted that the de-mixing of the separated phase into phases B and C is driven by the residual silica content in this liquid phase [86]. While the mechanism of secondary phase formation is still under investigation it is clear that it is a sequential process. Primary phase separation of a melt leads to the formation of two phases, referred to as phases X and Y in this example. Phase X represents the SiO_2 residual phase, and phase Y represents an alkaline earth borosilicate. Secondary phase separation causes phase Y to be further separated into two phases Y_1 and Y_2. In this step phase separation is driven by the coalescence of a SiO_2-rich phase Y_2 within a cation-rich borate phase Y_1 [88]. Compositionally Y_2 will be different from X, though both are rich in SiO_2.

While an increase in T_{PS} would affect primary phase separation, it is predicted that this would have subsequent effects on secondary phase formation if not by increasing the temperature of this transition, then by changing the viscosity of the various phases, which would alter the relaxation period needed for secondary phase formation and agglomeration. This is supported by the larger and more spherical phase C deposits observed for higher [MoO_3] or [B_2O_3], which implies that rearrangement and relaxation are occurring faster during cooling. As previously mentioned, increasing [MoO_3] or [B_2O_3] is also associated with an increased T_{PS}, which suggests a corresponding change to secondary phase formation. Furthermore, previous investigations have yielded that an increase in T_{PS} can decrease the fictive temperature (T_f) of the residual matrix [89], which is the point at which a liquid at metastable equilibrium transitions into a solid, and relaxation can no longer take place. This further indicates that increases in [MoO_3] or [B_2O_3] may increase the period available for primary and secondary phase formation and coalescence.

The second factor to determining why certain changes to morphology occurred is to understand how external radiation is interacting with matter, and how this mechanism of alteration may change depending on glass structure. There are two components to consider here. The first is the structural reorganization taking place from nuclear collisions, which can alter material properties [49, 60]. The second involves a thermal response from localized heating along ion tracks created by fast moving ions used during external irradiation. This effect is often described by the *thermal spike model*, which translates interactions of electrons in the target material with the irradiating ion to a small cylinder of energy with a characteristic temperature of ~1000 K [90]. In real systems undergoing α-decay these two processes can combine and result in an increase in T_f through a process of ballistic disorder (inclusive of melting) and fast quenching [61, 91]. This can subsequently remediate some phase separation, especially in systems with a higher T_{PS}.

4.2 Mechanism of radiation damage

Based on existing knowledge and results from this experiment, it hypothesized that the mechanism of alteration occurs in a three-step process: 1) the displacement of atoms through nuclear collision; 2) localized high temperature heating akin to melting at the collision site and along the ion track; 3) rapid quenching of these structural changes with the degree of alteration dependent on the composition of each phase.

The coalescence or segregation of particles is predicted to occur based on phase specific properties. Phases A, B and C are compositionally different and will therefore have a different packing factor, if this term is translated to an amorphous system. It is theorised that the varying densities within these phases will direct the ion interaction pathway, and therefore the accumulation of damage within each phase. When a high-energy ion impacts a surface it will hit some atom referred to as the primary knock-on atom (PKA). The depth that this ion will travel

before it collides with another atom will depend on its energy (and therefore speed), mass and charge. The PKA will then behave like a α-recoil and set off a billiard ball-type interaction, while the penetrating ion will continue travelling through the target material and initiate a series of additional displacement cascades interacting with target atoms at a higher frequency until it stops. As the ion travels along this pathway its electrons will also be interacting with the target material's electrons, creating a melt halo around every collision [92]. As the ion and knock-on atoms move through matter they will have a lower energy and will take the path of least resistance at a higher probability creating the most damage, in comparison to the higher energy PKA [93]. In heterogeneous systems, this means that the accumulated damage volume may vary from phase to phase characterised by varying compositions [59, 94]. It also means that the interface between phases where a density variation exists will be more susceptible to ion interactions. This has actually been thought to improve the radiation tolerance of multi-phase materials [95].

For systems without or with low [MoO_3], the allowable relaxation time correlated to $\Delta T = T_{PS} - T_g$ is shorter meaning that phases B and C will be compositionally more similar than if a longer relaxation time was available for additional SiO_2 to move out of phase B. Therefore, it is theorised that accumulated damage was more uniform within these phases, thus enabling a thermal relaxation type coalescence of phase C particles similar to that occurring during cooling [16]. For [MoO_3] $\geq$ 2.5mol%, which is associated with an increase in T_{PS} and thus a faster formation and relaxation of chemically different phases, a non-uniform response is expected. It is predicted that densification of phase C (Si-based droplets) and swelling of the phase B (cation and borate-rich matrix) takes place, as has been shown to occur in silicate and ternary glasses [49, 50, 96].

Given that the CB series had a fixed 2.5 mol% MoO_3 we would expect these glasses to behave in a similar manner, but it was observed that increasing [B_2O_3] to 23 mol% hindered this process of phase C densification and phase B expansion. Here it is theorised that the three dimensional connectivity of the borosilicate network provided improved elasticity to deformation and thus affected the thermal expansion coefficient. Based on ^{11}B MAS NMR results previously presented, synthesized CB23 showed a significantly higher fraction of BO_3 relative to $(BO_4)^-$ [65], with BO_3 groups primarily found as "ring" structures, as opposed to the higher fraction of "non-ring" seen for samples with [B_2O_3] ≤ 15mol% (see Electronic Supplementary Information). A higher concentration of these ring structures can be associated with restoring forces against deformation [97].

Testing of mechanical properties could be used as a first step to verify this theory. While performing ^{11}B MAS NMR was difficult on irradiated samples given the very small irradiation volume, other high-resolution techniques may be employed in future research for additional analysis and quantification of B_2O_3, which could not be accurately measured by EDS. This may provide greater insight and support the theories presented in this paper.

4.3 Direction of diffusion

In this study, EDS analysis was used to indicate how phases A, B, and C differed compositionally prior to and following irradiation. This yielded information of the migration of ions and the possible integration or segregation of phases occurring during irradiation. Two general trends could be identified. One was a surface-bulk diffusion of Ca, and occasionally Mo ions. The other was a cross phase diffusion of these ions with trends varying for the CB and CM series.

These were also the main mechanisms of modification observed following irradiation with β-particles [64] or Xe^{23+} ions [65], though variations in the direction of diffusion were observed with the type of irradiation. This is partly owing to β-irradiation remediating Si–O–B phase separation, whereas Xe-irradiation propagated de-mixing of the phases. These alterations were concurrent to different changes to the domain size of separated phases, with Au-irradiation producing the most significant modification. While some structural changes are attributed to composition and type of irradiation, the primary mechanism of cationic depletion at the surface is associate with an electric field gradient created by ions bombarding the surface [98, 99].

This side-effect to using external irradiation made cross-phase diffusion more difficult to analyse, but most interestingly the direction of this surface-bulk diffusion showed a dependency on composition. Samples with $[B_2O_3]$<20mol% exhibited bulk-to-surface precipitation, while surface-to-bulk ion depletion was observed for $[B_2O_3]$>20mol%. This multi-directional diffusion is hypothesized to be related to the relative $[(BO_4)^-]/[BO_3]$ at varying depths within the irradiation volume, as well as to the type of BO_3 structures. Previously published results suggest $[(BO_4)^-]/[BO_3]$ decrease as $[B_2O_3]$ increases . This is owing to a corresponding decrease in [CaO], thus promoting boron in its trigonal unit form [28] (see NMR spectra in Electronic Supplementary Information). Furthermore, an increased contribution from BO_3 units in ring structures, primarily boroxyl rings, over non-ring, which refers to trigonal boron distributed in silicate units [100], occurs as $[B_2O_3]$ increases [65]. This initial structure plays a role in the concentration of network-modifying cations and the degree of glass network connectivity.

The second factor to consider is that irradiation has previously been observed to cause a reduction in the coordination of boron that correspondingly increases the NBO population [49, 60, 101–103]. It is subsequently thought that in compositions with an initially higher $[(BO_4)^-]$ and with a

higher fraction of non-ring BO_3 units, newly dislodged cations to become trapped in depolymerised regions near the altered surface owing to a higher fraction of S–O–B linkages limiting mobility. In contrast, compositions with a higher [BO_3], and therefore increased phase separation through 2Si–O–B → B–O–B + Si–O–Si would have a more diffuse network and increased mobility of cations. This has similarly been observed to occur in sodium borosilicates under irradiation [98]. As a result, Au-irradiation primarily causes Ca depletion through a charged-based mechanism away from the surface. Further experimentation and analysis is required to prove this theory.

Reducing the [SiO_2]/[B_2O_3] also enabled the cleavage smaller single atom type rings and induced the formation of larger Si-O-B ones. This outlines the importance of B_2O_3 in controlling network connectivity and by extension the role of cations, which has a significant impact on the radiation response and mobility of ions. It may also affect the ability for certain phases to absorb incoming ionisation and therefore elicit precipitation versus ion depletion.

Independent of the type of diffusion, this process would first require the formation of ion migration channels. This can be achieved through accumulated ring cleavage between network formers, which creates NBOs. This type of bond cleavage can also modify the role of cations from network forming to network modifying. Together this can increase the diffusivity of ions, as has been previously observed to occur in irradiated glasses [32, 98].

While irradiation was generally observed to increase disorder within the molybdenum environment, thus enabling the increased integration of $(MoO_4)^{2-}$, the results in Figure 11 suggest that in pockets the opposite was true and these moieties clustered in depolymerised regions of the glass. The varied results suggest that radiation-induced diffusion of ions could contribute to both

phase separation and re-integration with a dependence of the initial properties of each phase. These properties also control the direction of ion diffusion between phases A/C ↔ B.

5.0 Conclusions

Several simplified calcium borosilicate glasses with varying [MoO_3] and [B_2O_3] were synthesised and irradiated with 7 MeV Au^{3+} ions used to simulate nuclear collisions resulting from the α-decay process. A dose of 3×10^{14} ions/cm^2 was achieved creating ~ 1 dpa of damage to a depth of 1.6 μm. Samples were then analysed using BSE imaging, EDS analysis, and Raman spectroscopy to identify factors affecting the chemistry of phase separation within heterogeneous glasses, and the solubility limit of problematic molybdenum groups. Radiation was observed to create several changes to the morphology, spatial distribution and size of separated phases within these three phased (A, B, and C) heterogeneous glasses. At low [MoO_3], phase C droplets were observed to coalesce into larger particles that became spherical emulating a temperature-based particle growth, whereas increasing [MoO_3] to 2.5mol% was observed to encourage droplet separation and segregation forming more evenly distributed particles. This latter type of segregation and distribution was also observable for compositions with [B_2O_3] ≤ 15mol% and is predicted to result from phase specific properties created from changes to T_{PS} and therefore the degree of heterogeneity. Increasing [B_2O_3] appeared to partially hinder this process owing to the initial defect structure, as well as significantly impacting the direction of ion diffusion. The process of surface-bulk and cross phase diffusion were enabled through increased disorder within the borosilicate network that increased the dissolution of $(MoO_4)^{2-}$ units in most areas based on damping of $(MoO_4)^{2-}$ Raman vibrational modes within a powellite-type structure, combined with growth of a band ~ 910 cm^{-1} associated with molybdate moieties dissolved into an amorphous

framework. Conclusions therefore report several effects of [MoO_3] and [B_2O_3] in directing structural modifications and altering the size of immiscible regions in multi-phase calcium borosilicate glasses following external Au-irradiation simulating α-decay on geological timescales.

Supporting Information. File "ESI.pdf" (PDF) contains TRIM calculations, compositional analysis (EDS and NMR) used to confer the validity of theoretical values listed in Table 1, additional EDS maps and Raman spectra.

Corresponding Author

*kp391@cam.ac.uk

Funding Sources

University of Cambridge, Department of Earth Sciences and EPSRC (Grant No. EP/K007882/1) for an IDS. Additional financial support provided by FfWG and the Cambridge Philosophical Society.

ACKNOWLEDGMENTS

The authors would like to thank Cyril Bachelet and the team at CSNSM for assistance with the irradiation experiment. They would also like to thank Sylvain Peuget for his assistance in initially driving the direction of this study and for useful discussions along the way. They would also like to acknowledge the help of several members in the Department of Earth Sciences (Robin Clarke, Chris Parish, Dr. Giulio Lampronti, and Dr. Iris Buisman) and those from the

Department of Material Science and Metallurgy (Lata Sahonta, Rachel Olivier) that aided in access to facilities and sample preparation, as well as training on analytical equipment.

ABBREVIATIONS

dpa displacement per atom, R7T7 French nuclear waste glass composition, SON68 inactive version of R7T7, GC glass ceramic, T_{PS} phase separation temperature, T_f fictive temperature, NBO non-bridging oxygen.

REFERENCES

1. Lee WE, Ojovan MI, Stennett MC, Hyatt NC. Immobilisation of radioactive waste in glasses, glass composite materials and ceramics. *Adv Appl Ceram*. 2006;105(1):3–12. https://doi.org/10.1179/174367606X81669

2. Peuget S, Cachia J-N, Jégou C, *et al.* Irradiation stability of R7T7-type borosilicate glass. *J Nucl Mater*. 2006;354(1–3):1–13. https://doi.org/10.1016/j.jnucmat.2006.01.021

3. Frugier P, Martin C, Ribet I, Advocat T, Gin S. The effect of composition on the leaching of three nuclear waste glasses: R7T7, AVM and VRZ. *J Nucl Mater*. 2005;346(2–3):194–207. https://doi.org/10.1016/j.jnucmat.2005.06.023

4. Gin S, Guittonneau C, Godon N, *et al.* Nuclear glass durability: New insight into alteration layer properties. *J Phys Chem C*. 2011;115(38):18696–18706. https://doi.org/10.1021/jp205477q

5. IAEA. Storage and Disposal of Spent Fuel and High Level Radioactive Waste. 2006

6. Weber WJ, Ewing RC, Angell CA, *et al.* Radiation effects in glasses used for immobilization of high-level waste and plutonium disposition. *J Mater Res*. 1997;12(8):1946–1978. https://doi.org/10.1557/JMR.1997.0266

7. Gras JM, Quang R Do, Masson H, *et al.* Perspectives on the closed fuel cycle - Implications for high-level waste matrices. *J Nucl Mater*. 2007;362(2–3):383–394. https://doi.org/10.1016/j.jnucmat.2007.01.210

8. Weber WJ, Navrotsky A, Stefanovsky S, Vance ER, Vernaz E. Materials Science of High-Level Nuclear Waste Immobilization. *MRS Bull*. 2009;34(1):46–53. https://doi.org/10.1557/mrs2009.12

9. Calas G, Le Grand M, Galoisy L, Ghaleb D. Structural role of molybdenum in nuclear glasses: an EXAFS study. *J Nucl Mater*. 2003;322:15–20. https://doi.org/10.1016/S0022-3115(03)00277-0

10. Horneber A, Camara B, Lutze W. Investigation on the Oxidation State and The Behaviour of Molybdenum in Silicate Glass. *MRS Proc Sci Basis Nucl Waste Manag V*. 1982;11:279–288. https://doi.org/10.1557/PROC-11-279

11. Nicoleau E, Schuller S, Angeli F, *et al.* Phase separation and crystallization effects on the structure and durability of molybdenum borosilicate glass. *J Non Cryst Solids*. 2015;427:120–133. https://doi.org/10.1016/j.jnoncrysol.2015.07.001

12. Magnin M, Schuller S, Mercier C, *et al.* Modification of molybdenum structural environment in borosilicate glasses with increasing content of boron and calcium oxide by 95Mo MAS NMR. *J Am Ceram Soc*. 2011;94(12):4274–4282. https://doi.org/10.1111/j.1551-2916.2011.04919.x

13. Vance ER, Davis J, Olufson K, *et al.* Leaching behaviour of and Cs disposition in a UMo powellite glass-ceramic. *J Nucl Mater*. 2014;448(1–3):325–329. https://doi.org/10.1016/j.jnucmat.2014.02.024

14. Crum J V., Riley BJ, Turo LR, Tang M, Kossoy A. Summary Report: Glass-Ceramic Waste Forms for Combined Fission Products. Richland: 2011

15. Dunnett BF, Gribble NR, Short R, Turner E, Steele CJ, Riley AD. Vitrification of high molybdenum waste. *Glas Technol Eur J Glas Sci Technol Part A*. 2012;53(4):166–171.

16. Schuller S, Pinet O, Grandjean A, Blisson T. Phase separation and crystallization of borosilicate glass enriched in MoO3, P2O5, ZrO2, CaO. *J Non Cryst Solids*. 2008;354(2–9):296–300. https://doi.org/10.1016/j.jnoncrysol.2007.07.041

17. Ojovan MI, Lee WE, Ion SE. An Introduction to Nuclear Waste Immobilisation. Elsevier; 2005 https://doi.org/10.1016/B978-008044462-8/50000-4

18. Haynes WM. CRC Handbook of Chemistry and Physics. 94th ed. CRC Press; 2013

19. Caurant D, Majérus O, Fadel E, Lenoir M, Gervais C, Pinet O. Effect of molybdenum on the structure and on the crystallization of SiO2-Na2O-CaO-B2O3 glasses. *J Am Ceram Soc*. 2007;90(3):774–783. https://doi.org/10.1111/j.1551-2916.2006.01467.x

20. Short RJ, Hand RJ, Hyatt NC, Möbus G. Environment and oxidation state of molybdenum in simulated high level nuclear waste glass compositions. *J Nucl Mater*. 2005;340:179–186. https://doi.org/10.1016/j.jnucmat.2004.11.008

21. Chouard N, Caurant D, Majérus O, *et al.* Effect of MoO3, Nd2O3, and RuO2 on the crystallization of soda–lime aluminoborosilicate glasses. *J Mater Sci*. 2015;50(1):219–241. https://doi.org/10.1007/s10853-014-8581-9

22. Greaves GN, Sen S. Inorganic glasses, glass-forming liquids and amorphizing solids. *Adv Phys*. 2007;56(1):1–166. https://doi.org/10.1080/00018730601147426

23. Caurant D, Majérus O, Fadel E, *et al.* Structural investigations of borosilicate glasses containing MoO3 by MAS NMR and Raman spectroscopies. *J Nucl Mater*. 2010;396(1):94–101. https://doi.org/10.1016/j.jnucmat.2009.10.059

24. Short RJ, Hand RJ, Hyatt NC, Möbus G. Environment and oxidation state of molybdenum in simulated high level nuclear waste glass compositions. *J Nucl Mater*. 2005;340(2–3):179–186. https://doi.org/10.1016/j.jnucmat.2004.11.008

25. Huang M, Johns JR, Howe RF. EPR study of the superoxide ion in molybdenum zeolites. *J Phys Chem*. 1988;92(5):1291–1295. https://doi.org/10.1021/j100316a055

26. Christofilos D, Kourouklis GA, Ves S. A high pressure Raman study of calcium molybdate. *J Phys Chem Solids*. 1995;56(8):1125–1129. https://doi.org/10.1016/0022-3697(95)00034-8

27. Yun YH, Bray PJ. Nuclear magnetic resonance studies of the glasses in the system K2OB2O3P2O5. *J Non Cryst Solids*. 1978;27:363–380. https://doi.org/10.1016/0022-3093(78)90055-8

28. Navrotsky A, Geisinger KL, Gibbs G V. The Tetrahedral Framework in Glasses and M e l t s - Inferences from Molecular Orbital Calculations and Implications for Structure , Thermodynamics , and Physical Properties. *Phys Chem Miner*. 1985;11:284–298.

29. Möncke D, Tricot G, Winterstein-Beckmann, Anja Wondraczek L, Kamitsos EI. On the connectivity of borate tetrahedra in borate and borosilicate glasses. *Eur J Glas Sci Technol Part B Phys Chem Glas*. 2015;56(5):203–211. https://doi.org/10.13036/17533562.56.5.203

30. Manara D, Grandjean A, Neuville DR. Structure of borosilicate glasses and melts: A revision of the Yun, Bray and Dell model. *J Non Cryst Solids*. 2009;355(50–51):2528–2531. https://doi.org/10.1016/j.jnoncrysol.2009.08.033

31. Manara D, Grandjean A, Neuville DR. Advances in understanding the structure of borosilicate glasses: A raman spectroscopy study. *Am Mineral*. 2009;94(5–6):777–784. https://doi.org/10.2138/am.2009.3027

32. Battaglin G, Arnold GW, Mattei G, Mazzoldi P, Dran J-C. Structural modifications in ion-implanted silicate glasses. *J Appl Phys*. 1999;85(12):8040–8049. https://doi.org/10.1063/1.370640

33. Hehlen B, Neuville DR. Raman response of network modifier cations in alumino-silicate glasses. *J Phys Chem B*. 2015;119(10):4093–4098. https://doi.org/10.1021/jp5116299

34. Du LS, Stebbins JF. Solid-state NMR study of metastable immiscibility in alkali borosilicate glasses. *J Non Cryst Solids*. 2003;315(3):239–255. https://doi.org/10.1016/S0022-3093(02)01604-6

35. Smedskjaer MM, Zheng Q, Mauro JC, Potuzak M, Mørup S, Yue Y. Sodium diffusion in boroaluminosilicate glasses. *J Non Cryst Solids*. 2011;357(22–23):3744–3750. https://doi.org/10.1016/j.jnoncrysol.2011.07.008

36. Greaves GN, Ngai KL. Reconciling ionic-transport properties with atomic structure in oxide glasses. *Phys Rev B*. 1995;52(9):6358–6380. https://doi.org/10.1103/PhysRevB.52.6358

37. Du L-S, Stebbins JF. Network connectivity in aluminoborosilicate glasses: A high-resolution 11 B, 27 Al and 17 O NMR study. *J Non Cryst Solids*. 2005;351(9):3508–3520.

38. Calas G, Galoisy L, Cormier L, Ferlat G, Lelong G. The Structural Properties of Cations in Nuclear Glasses. *Procedia Mater Sci*. 2014;7:23–31. https://doi.org/10.1016/j.mspro.2014.10.005

39. Hudon P, Baker DR. The nature of phase separation in binary oxide melts and glasses . I . Silicate systems. *J Non Cryst Solids*. 2002;303:299–345.

40. Lee SK, Stebbins JF. Nature of cation mixing and ordering in Na-Ca silicate glasses and melts. *J Phys Chem B*. 2003;107(14):3141–3148. https://doi.org/10.1021/jp027489y

41. Martineau C, Michaelis VK, Schuller S, Kroeker S. Liquid-liquid phase separation in model nuclear waste glasses: A solid-state double-resonance NMR study. *Chem Mater*. 2010;22(17):4896–4903. https://doi.org/10.1021/cm1006058

42. Chouard N, Caurant D, Majérus O, *et al.* Effect of neodymium oxide on the solubility of MoO3 in an aluminoborosilicate glass. *J Non Cryst Solids*. 2011;357(14):2752–2762. https://doi.org/10.1016/j.jnoncrysol.2011.02.015

43. Taurines T, Boizot B. Microstructure of powellite-rich glass-ceramics: A model system for high level waste immobilization. *J Am Ceram Soc*. 2012;95(3):1105–1111. https://doi.org/10.1111/j.1551-2916.2011.05015.x

44. Henry N, Deniard P, Jobic S, *et al.* Heat treatments versus microstructure in a molybdenum-rich borosilicate. *J Non Cryst Solids*. 2004;333(2):199–205. https://doi.org/10.1016/j.jnoncrysol.2003.09.055

45. Kawamoto Y, Clemens K, Tomozawa M. Effects of MoO3 on phase separation of Na20-B203-Si02 glasses. *J Am Ceram Soc*. 1981;64(5):292–296. https://doi.org/10.1111/j.1151-2916.1981.tb09605.x

46. Ishiguro K, Kawanishi N, Nagaki H, Naito A. Chemical states of molybdenum in radioactive waste glass (PNCT-N--831-82-01). Tokyo, Japan: 1982 https://doi.org/PNCT-N--831-82-01

47. Quintas A, Caurant D, Majérus O, Charpentier T, Dussossoy JL. Effect of compositional variations on charge compensation of AlO4 and BO4 entities and on crystallization tendency of a rare-earth-rich aluminoborosilicate glass. *Mater Res Bull*. 2009;44(9):1895–1898. https://doi.org/10.1016/j.materresbull.2009.05.009

48. Morey GW, Ingerson E. The melting of danburite: a study of liquid immiscibility in the system, CaO-B2O3-SiO2. *Am Mineral*. 1937;22(1):37–47.

49. Peuget S, Delaye JM, Jégou C. Specific outcomes of the research on the radiation stability of the French nuclear glass towards alpha decay accumulation. *J Nucl Mater*. 2014;444(1–3):76–91. https://doi.org/10.1016/j.jnucmat.2013.09.039

50. Delaye J-M, Peuget S, Bureau G, Calas G. Molecular dynamics simulation of radiation damage in glasses. *J Non Cryst Solids*. 2011;357(14):2763–2768. https://doi.org/10.1016/j.jnoncrysol.2011.02.026

51. Boizot B, Petite G, Ghaleb D, Calas G. Radiation induced paramagnetic centres in nuclear glasses by EPR spectroscopy. *Nucl Instruments Methods Phys Res Sect B Beam Interact with Mater Atoms*. 1998;141(1–4):580–584. https://doi.org/10.1016/S0168-583X(98)00102-5

52. Inagaki Y, Furuya H, Idemitsu K. Microstructure of simulated high-level waste glass doped with short-lived actinides, 238Pu and 244Cm. *Mat Res Soc Symp Proc*. 1992;257:199–206. https://doi.org/10.1557/PROC-257-199

53. Ewing RC, Meldrum A, Wang L, Wang S. Radiation-Induced Amorphization. *Rev Mineral Geochemistry*. 2000;39(1):319–361. https://doi.org/10.2138/rmg.2000.39.12

54. Peng HB, Sun ML, Yang KJ, *et al.* Effect of irradiation on hardness of borosilicate glass. *J Non Cryst Solids*. 2016;443:143–147. https://doi.org/10.1016/j.jnoncrysol.2016.04.027

55. Kieffer J. Structural Transitions and Glass Formation. *J Phys Chem B*. 1999;103:4153–4158. https://doi.org/10.1021/jp984092e

56. Yazawa T, Kuraoka K, Akai T, Umesaki N, Du W. Clarification of Phase Separation Mechanism of Sodium Borosilicate Glasses in Early Stage by Nuclear Magnetic Resonance. *J Phys Chem B*. 2000;104:2109–2116. https://doi.org/10.1021/jp993416b

57. Martel L, Allix M, Millot F, *et al.* Controlling the size of nanodomains in calcium aluminosilicate glasses. *J Phys Chem C*. 2011;115(39):18935–18945. https://doi.org/10.1021/jp200824m

58. Zhang Y, Bae IT, Sun K, *et al.* Damage profile and ion distribution of slow heavy ions in compounds. *J Appl Phys*. 2009;105(104901). https://doi.org/10.1063/1.3118582

59. Ziegler JF, Ziegler MD, Biersack JP. SRIM - The stopping and range of ions in matter (2010). *Nucl Instruments Methods Phys Res B Beam Interact with Mater Atoms*. 2010;268(11–12):1818–1823. https://doi.org/10.1016/j.nimb.2010.02.091

60. Bonfils J de, Peuget S, Panczer G, *et al.* Effect of chemical composition on borosilicate glass behavior under irradiation. *J Non Cryst Solids*. 2010;356(6–8):388–393. https://doi.org/10.1016/j.jnoncrysol.2009.11.030

61. Maugeri EA, Peuget S, Staicu D, Zappia A, Jegou C, Wiss T. Calorimetric study of glass structure modification induced by α decay. *J Am Ceram Soc*. 2012;95(9):2869–2875. https://doi.org/10.1111/j.1551-2916.2012.05304.x

62. Schuller S, Pinet O, Penelon B. Liquid-liquid phase separation process in borosilicate liquids enriched in molybdenum and phosphorus oxides. *J Am Ceram Soc*. 2011;94(2):447–454. https://doi.org/10.1111/j.1551-2916.2010.04131.x

63. Brehault A, Patil D, Kamat H, *et al.* Compositional Dependence of Solubility/Retention of Molybdenum Oxides in Aluminoborosilicate-Based Model Nuclear Waste Glasses. *J Phys Chem B*. 2018;122:1714–1729. https://doi.org/10.1021/acs.jpcb.7b09158

64. Patel KB, Boizot B, Facq SP, Peuget S, Schuller S, Farnan I. Impacts of composition and beta irradiation on phase separation in multiphase amorphous calcium borosilicates. *J Non Cryst Solids*. 2017;473:1–16. https://doi.org/10.1016/j.jnoncrysol.2017.06.018

65. Patel KB, Peuget S, Schuller S. Swift heavy ion-irradiated multi-phase calcium borosilicates : implications to molybdenum incorporation , microstructure , and network topology. *J Mater Sci*. 2019;54(18):11763–11783. https://doi.org/10.1007/s10853-019-03714-2

66. Was GS, Averback RS. Radiation damage using ion beams. Elsevier Inc.; 2012 https://doi.org/10.1016/B978-0-08-056033-5.00007-0

67. Liu Y, Han X, Crespillo ML, Huang Q, Liu P, Wang X. Ion tracks formation through synergistic energy processes in strontium titanate under swift heavy ion irradiation: Experimental and theoretical approaches. *Materialia*. 2019;7(March):100402. https://doi.org/10.1016/j.mtla.2019.100402

68. Neuville DR, Cormier L, Boizot B, Flank AM. Structure of β-irradiated glasses studied by X-ray absorption and Raman spectroscopies. *J Non Cryst Solids*. 2003;323:207–213. https://doi.org/10.1016/S0022-3093(03)00308-9

69. Manghnani MH, Hushur A, Sekine T, Wu J, Stebbins JF, Williams Q. Raman, Brillouin, and nuclear magnetic resonance spectroscopic studies on shocked borosilicate glass. *J Appl Phys*. 2011;109(11). https://doi.org/10.1063/1.3592346

70. Furukawa T, White WB. Raman spectroscopic investigation of sodium borosilicate glass structure. *J Mater Sci*. 1981;16(10):2689–2700. https://doi.org/10.1007/BF00552951

71. Walrafen GE, Samanta SR, Krishnan PN. Raman investigation of vitreous and molten boric oxide. *J Chem Phys*. 1980;72(1):113–120. https://doi.org/10.1063/1.438894

72. Konijnendijk WL, Stevels JM. The structure of borate glasses studied by Raman scattering. *J Non Cryst Solids*. 1975;18(3):307–331. https://doi.org/10.1016/0022-3093(75)90137-4

73. Krogh-Moe J. The structure of vitreous and liquid boron oxide. *J Non Cryst Solids*. 1969;1:269–284. https://doi.org/10.1016/0022-3093(69)90025-8

74. Yano T, Kunimine N, Shibata S, Yamane M. Structural investigation of sodium borate glasses and melts by Raman spectroscopy. I. Quantitative evaluation of structural units. *J Non Cryst Solids*. 2003;321(3):137–146. https://doi.org/10.1016/S0022-3093(03)00158-3

75. Frost RL, Bouzaid J, Butler IS. Raman spectroscopic study of the molybdate mineral szenicsite and com- pared with other paragenetically related molybdate minerals. *Spectrosc Lett*. 2007;40(4):603–614. https://doi.org/10.1002/jrs.820

76. Wang X, Panczer G, de Ligny D, *et al.* Irradiated rare-earth-doped powellite single crystal probed by confocal Raman mapping and transmission electron microscopy. *J Raman Spectrosc*. 2014;45:383–391. https://doi.org/10.1002/jrs.4472

77. Debenedetti PG, Stillinger FH. Review article Supercooled liquids and the glass transition. *Nature*. 2001;410(March):259.

78. Liu H, Youngman RE, Kapoor S, Jensen LR, Smedskjaer MM, Yue Y. Nano-phase separation and structural ordering in silica-rich mixed network former glasses. *Phys Chem Chem Phys*. 2018;20:15707–15717. https://doi.org/10.1039/c8cp01728j

79. Wheaton BR, Clare AG. Evaluation of phase separation in glasses with the use of atomic force microscopy. *J Non Cryst Solids*. 2007;353:4767–4778. https://doi.org/10.1016/j.jnoncrysol.2007.06.073

80. Du WF, Kuraoka K, Akai T, Yazawa T. Study of kinetics of the phase separation in sodium borate glasses. *J Mater Sci*. 2000;35:3913–3921. https://doi.org/10.1023/A:1004845817600

81. Sickafus KE, Grimes RW, Valdez JA, *et al.* Radiation-induced amorphization resistance and radiation tolerance in structurally related oxides. *Nat Mater*. 2007;6:217–223. https://doi.org/10.1038/nmat1842

82. Lian J, Wang LM, Ewing RC, Yudintsev S V, Stefanovsky S V. Thermally induced phase decomposition and nanocrystal formation in murataite ceramics. *J Mater Chemsitry*. 2004;15:709–714. https://doi.org/10.1039/b411845f

83. Hobbs LW, Clinard FW, Zinkle SJ, Ewing RC. Radiation effects in ceramics. *J Nucl Mater*. 1994;216(C):291–321. https://doi.org/10.1016/0022-3115(94)90017-5

84. Zaitsev AI, Shelkova NE, Mogutnov BM. Thermodynamics of Na2O-SiO2 Melts. *Inorg Mater*. 2000;36(6):529–543.

85. Mazurin O V. Physcial Properties of Phase Separated Glasses. *J Non Cryst Solids*. 1987;95&96:71–82.

86. Vogel W. Glass Chemistry. 2nd ed. Berlin Heidelberg: Springer-Verlag; 1994 https://doi.org/10.1007/978-3-642-78723-2

87. Kroeker S, Schuller S, Wren JEC, Greer BJ, Mesbah A. 133Cs and 23Na MAS NMR Spectroscopy of Molybdate Crystallization in Model Nuclear Glasses. *J Am Ceram Soc*. 2016;99(5):1557–1564. https://doi.org/10.1111/jace.14082

88. Schuller S. Phase separation processes in glass. In: Neuville DR, Cornier L, Caurant D, Montagne L, eds. *From Glas. to Cryst.* EDP Sciences; 2017:125–150.

89. Kobayashi H, Takahashi H. Roles of intermediate-range orders on the glass transition process: Fictive temperature, residual entropy, relaxation time and boson peak. *J Non Cryst Solids*. 2015;427:34–40. https://doi.org/10.1016/j.jnoncrysol.2015.06.029

90. Toulemonde M, Dufour C, Paumier E. Transient thermal process after a high-energy heavy-ion irradiation of amorphous metals and semiconductors. *Phys Rev B*. 1992;46(22):14362–14369. https://doi.org/10.1103/PhysRevB.46.14362

91. Griscom DL, Weber WJ. Electron spin resonance study of Fe3+ and Mn2+ ions in 17-year-old nuclear-waste-glass simulants containing PuO2 with different degrees of 238Pu substitution. *J Non Cryst Solids*. 2011;357(5):1437–1451. https://doi.org/10.1016/j.jnoncrysol.2010.11.017

92. García G, Rivera A, Crespillo ML, Gordillo N, Olivares J, Agulló-López F. Amorphization kinetics under swift heavy ion irradiation: A cumulative overlapping-track approach. *Nucl Instruments Methods Phys Res Sect B Beam Interact with Mater Atoms*. 2011;269(4):492–497. https://doi.org/10.1016/j.nimb.2010.12.073

93. Olander DR. Fundamental Aspects of Nuclear Reactor Fuel Elements. US Energy Research and Development Administration; 1976

94. Hirata K, Kobayashi Y, Hishita S, Ujihira Y. Damage depth-profiling of Au and O-irradiated amorphous PEEK by monoenergetic positron beams. *Appl Phys A*. 1997;64(5):491–495. https://doi.org/10.1007/s003390050507

95. Ohtaki KK, Patel MK, Crespillo ML, Karandikar KK. Improved high temperature radiation damage tolerance in a three-phase ceramic with heterointerfaces. *Sci Rep*. 2018;8(13993). https://doi.org/10.1038/s41598-018-31721-x

96. Devine RAB. Macroscopic and microscopic effects of radiation in amorphous SiO2. *Nucl Instruments Methods Phys Res Sect B Beam Interact with Mater Atoms*. 1994;91(1–4):378–390. https://doi.org/10.1016/0168-583X(94)96253-7

97. Wang W, Christensen R, Curtis B, Martin SW, Kieffer J. A new model linking elastic properties and ionic conductivity of mixed network former glasses. *Phys Chem Chem Phys*. 2018;20(3):1629–1641.

98. Mir AH, Boizot B, Charpentier T, *et al.* Surface and bulk electron irradiation effects in simple and complex glasses. *J Non Cryst Solids*. 2016;453:141–149. https://doi.org/10.1016/j.jnoncrysol.2016.10.009

99. Boizot B, Petite G, Ghaleb D, *et al.* Migration and segregation of sodium under β-irradiation in nuclear glasses. *Nucl Instruments Methods Phys Res B Beam Interact with Mater Atoms*. 2000;166–167:500–504. https://doi.org/10.1016/S0168-583X(99)00787-9

100. Du L, Stebbins JF. 11B Nature of Silicon - Boron Mixing in Sodium Borosilicate Glasses : A High-Resolution and 17O NMR Study. *J Phys Chem B*. 2003;107:10063–10076. https://doi.org/10.1021/jp034048l

101. Boizot B, Ollier N, Olivier F, Petite G, Ghaleb D, Malchukova E. Irradiation effects in simplified nuclear waste glasses. *Nucl Instruments Methods Phys Res Sect B Beam Interact with Mater Atoms*. 2005;240(1–2):146–151. https://doi.org/10.1016/j.nimb.2005.06.105

102. Charpentier T, Martel L, Mir AH, Somers J, Jégou C, Peuget S. Self-healing capacity of nuclear glass observed by NMR spectroscopy. *Sci Rep*. 2016;6(1):25499. https://doi.org/10.1038/srep25499

103. Chen L, Yuan W, Nan S, *et al.* Study of modifications in the mechanical properties of sodium aluminoborosilicate glass induced by heavy ions and electrons. *Nucl Instruments Methods Phys Res Sect B Beam Interact with Mater Atoms*. 2016;370:42–48. https://doi.org/10.1016/j.nimb.2016.01.007

Table 1. Theoretical batch sample composition in mol%.

Series	Sample ID	SiO_2	B_2O_3	CaO	MoO_3	Gd_2O_3
CB	CB7	78.07	7.00	12.28	2.50	0.15
	CB15	71.16	15.00	11.19	2.50	0.15
	CB23	64.16	23.00	10.09	2.50	0.15
CM	CaBSi	67.74	20.97	11.29	-	-
	CM1	67.07	20.76	11.18	1.00	-
	CM2.5	66.05	20.44	11.01	2.50	-
	CM7	63.00	19.50	10.50	7.00	-

Table 2. Calculated [Si]/[Ca] and [Ca]/[Mo] ratios for phases A, B and C before and after irradiation.

Sample	Dose	Phase A		Phase B		Phase C	
	(ions/cm^2)	Si/Ca	Ca/Mo	Si/Ca	Ca/Mo	Si/Ca	Ca/Mo
CB7	0	63.032 (± 3.753)	1.137 (± 0.515)	8.233 (± 0.451)	1.557 (± 0.116)	44.501 (± 2.687)	0.931 (± 0.256)
	3×10^{14}	44.475 (± 5.314)	8.972 (± 1.271)	2.235 (± 0.112)	5.412 (± 0.140)	24.922 (± 2.608)	7.201 (± 0.434)
CB15	0	53.976 (± 3.833)	2.586 (± 0.237)	2.671 (± 0.250)	4.300 (± 0.296)	13.654 (± 1.006)	8.439 (± 0.452)
	3×10^{14}	28.452 (± 3.392)	6.175 (± 0.609)	2.257 (± 0.114)	4.450 (± 0.273)	11.460 (± 1.667)	6.569 (± 1.780)
CB23	0	32.220 (± 0.417)	4.186 (± 0.646)	2.096 (± 0.056)	5.339 (± 0.082)	10.610 (± 0.154)	2.850 (± 0.196)
	3×10^{14}	56.176 (± 1.270)	3.456 (± 1.193)	2.716 (± 0.082)	3.011 (± 0.110)	18.265 (± 0.425)	2.823 (± 0.579)
CaBSi	0	58.263 (± 1.305)	-	2.035 (± 0.128)	-	9.237 (± 2.031)	-
	3×10^{14}	46.647 (± 5.547)	-	2.542 (± 0.099)	-	5.291 (± 0.173)	-
CM1	0	40.426 (± 0.710)	3.862 (± 0.116)	2.627 (± 0.155)	19.391 (± 0.423)	9.223 (± 1.715)	13.362 (± 0.260)
	3×10^{14}	58.226 (± 5.035)	19.532 (± 6.082)	3.477 (± 0.136)	32.031 (± 0.052)	10.179 (± 0.831)	19.609 (± 0.097)
CM2.5	0	59.810 (± 1.837)	3.851 (± 0.308)	1.350 (± 0.104)	5.127 (± 0.494)	15.098 (± 0.509)	6.505 (± 0.835)
	3×10^{14}	53.890 (± 1.754)	2.230 (± 0.237)	2.216 (± 0.103)	5.255 (± 0.273)	7.334 (± 0.565)	6.685 (± 0.898)
CM7*	0	54.510 (± 2.415)	0.346 (± 0.516)	2.610 (± 0.410)	1.340 (± 0.221)	-	-
	3×10^{14}	47.379 (± 3.701)	2.141 (± 0.725)	3.168 (± 0.104)	1.351 (± 0.062)	-	-

*CM7 is a GC not a heterogeneous glass; therefore phase B represents the crystalline phase.

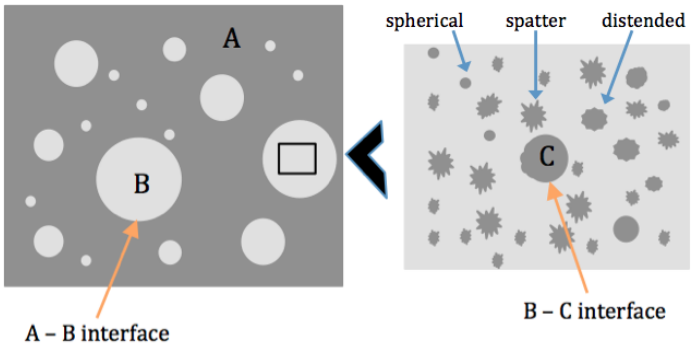

Figure 1. Schematic of embedded immiscibility within synthesised calcium borosilicates [50]. Phase A is a Si-rich residual phase within which heterogeneously distributed phase B deposits rich in Ca/Mo and of varying size are located. Within these deposits are smaller phase C droplets, which are found to form in a variety of geometries as labelled above.

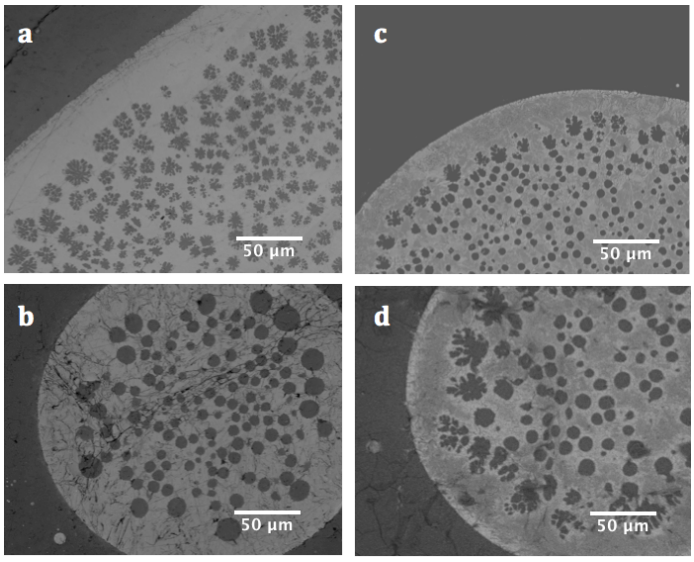

Figure 2. BSE images of CB15 (a) prior to, and (c) following irradiation; and of CB23 (b) prior to, and (d) following irradiation with Au ions.

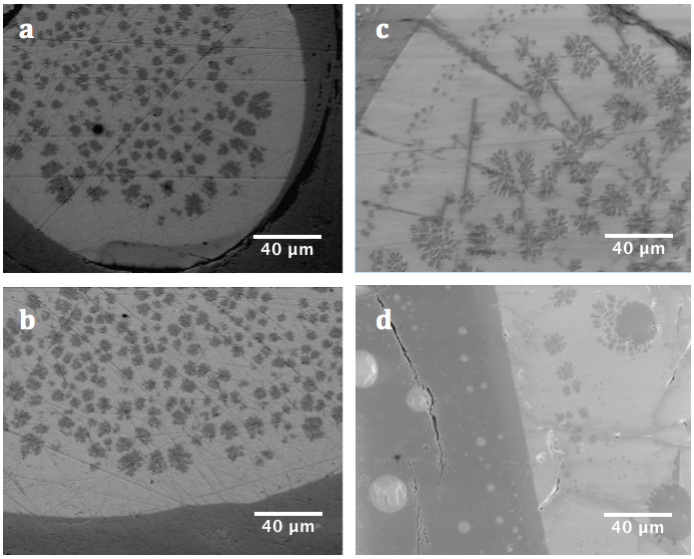

Figure 3. BSE images of CaBSi: (a) & (b) at pristine conditions, and (c) & (d) following Au-irradiation. These images reveal an array of structural features, and the variance in the domain size of separated phases before and after irradiation. It is evident from these images that Au-irradiation was observed to cause several changes to the size and distribution of phase C droplets.

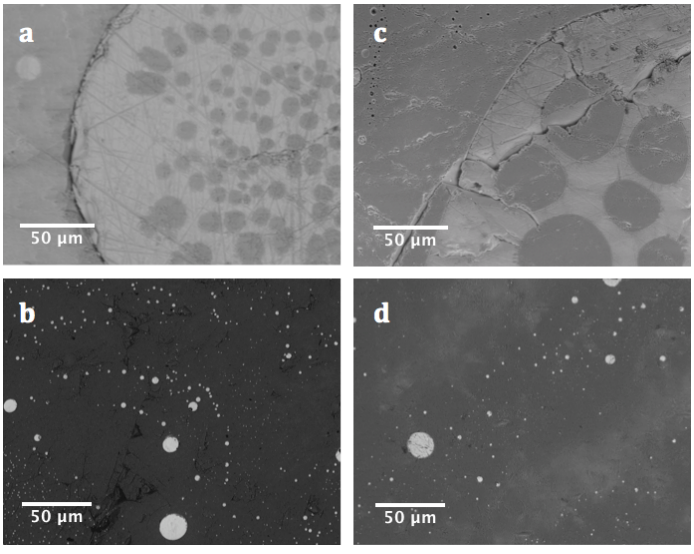

Figure 4. BSE images of the multi-amorphous phased CM1 (a) prior to, and (c) following irradiation; and of the glass ceramic CM7 (b) prior to, and (d) following Au-irradiation.

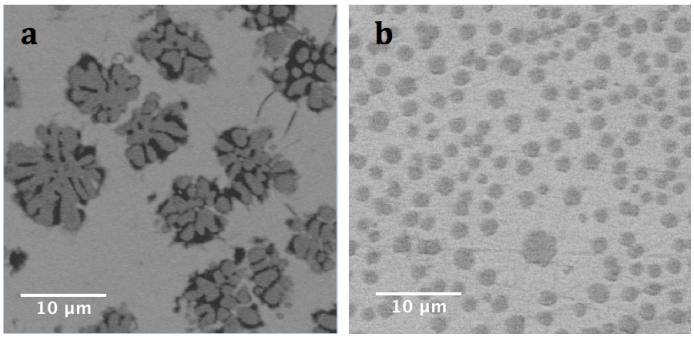

Figure 5. BSE images of phase C droplets within phase B of CM2.5: (a) following synthesis, and (b) following irradiation with Au ions.

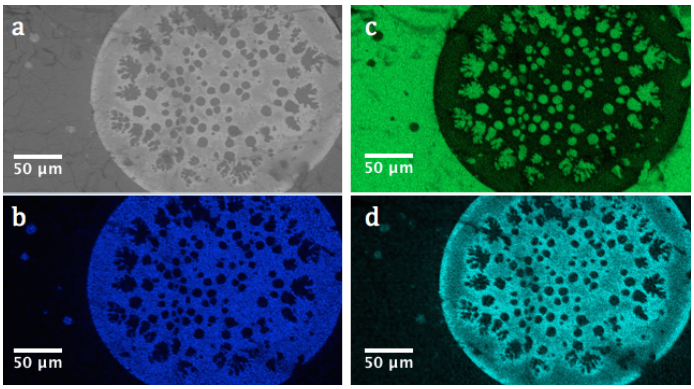

Figure 6. EDS maps of CB23 irradiated with Au ions showing three immiscible phases with the interface between phases enriched in Mo/Ca. Several areas from each phase within these maps were used for the calculations in Table 2. Micrographs are as follows: a) BSE image (grey), b) Ca (blue), c) Si (green), and d) Mo (aqua).

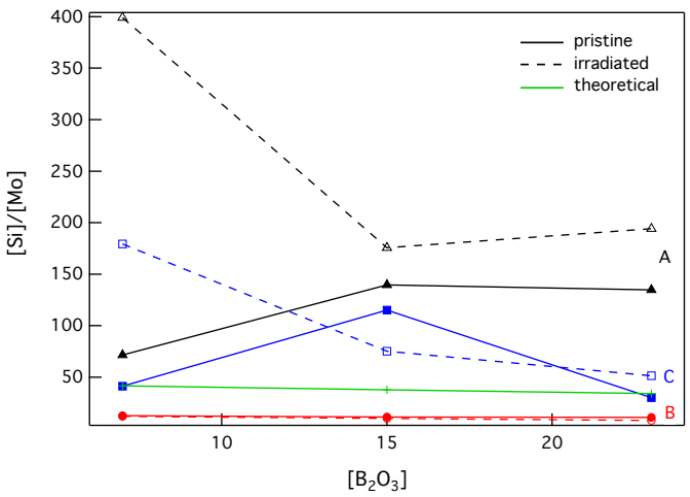

Figure 7. [Si]/[Mo] trends in phase A (black), B (red) and C (blue) for samples in the CB series prior to (solid lines), and following irradiation (dashed lines). The theoretical batch sample composition is also provided for comparison.

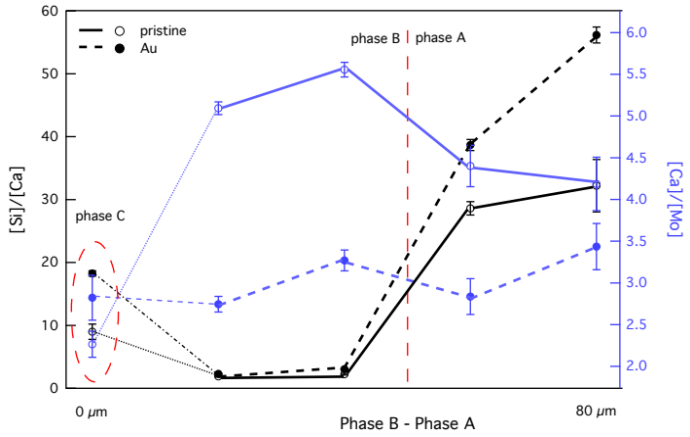

Figure 8. [Si]/[Ca] (black lines) and [Ca]/[Mo] (blue lines) ratios across the B–C and A–B interfaces in CB23 prior to (solid lines) and following irradiation with Au ions (dashed lines).

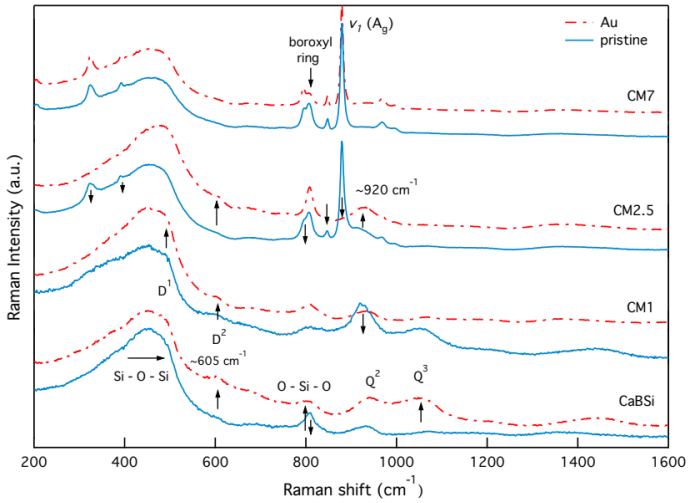

Figure 9. Raman spectra of samples in the CM series prior to (blue solid line), and following irradiation (red dashed line). Bands of interest have been labelled, as well as radiation-induced shifts.

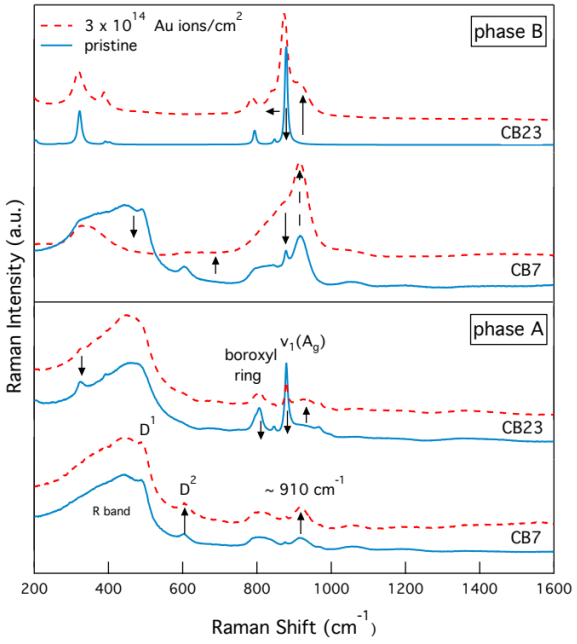

Figure 10. Raman spectra of the Si-rich phase A (bottom half) and the Ca/Mo-rich phase B (top half) of CB7 and CB23 prior to (blue solid line) and following Au-irradiation (red dashed line).

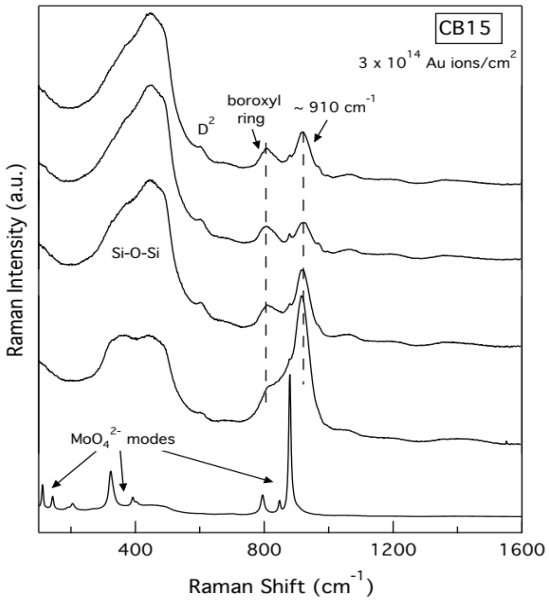

Figure 11. Raman spectra indicating multiple phases, or mixed regions of CB15 following Au-irradiation. The spectrum at the bottom is Mo-rich showing contributions primarily from MoO_4^{2-} vibrational bands. Each additional spectrum shows a larger silicate contribution until the top, which represents phase A. These spectra show an evolution of MoO_4^{2-} oxyanion migration, likely occurring through a mixing of phases A and B or of phases B and C.

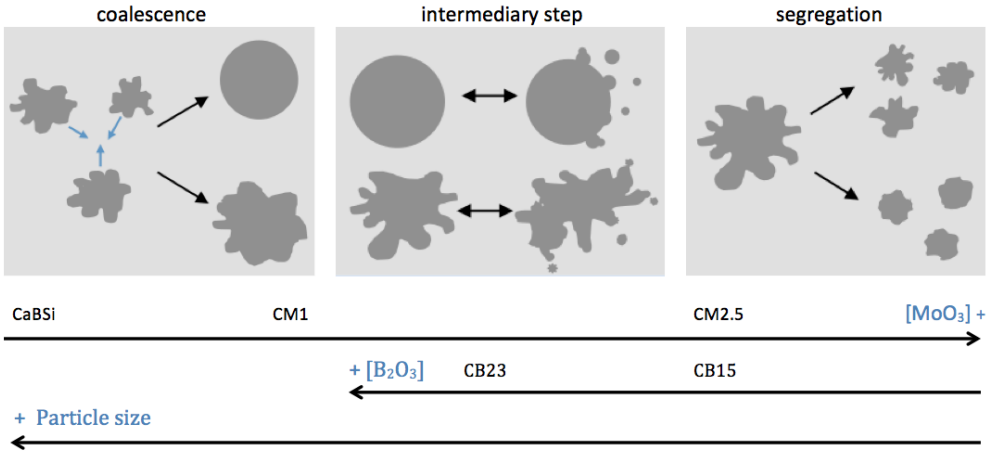

Figure 12. Compositional dependent mechanisms of modification for immiscible phase C following Au-irradiation. Direction of arrow represents increasing value of concentration or particle size. Coalescence is akin to temperature-based particle growth, while segregation is related to radiation-induced disorder.

Table of Contents (TOC)/Graphical Abstract